DEVICES FOR FATIGUE TESTING OF ELECTROPLATED NICKEL (MEMS)

Kristian. P. Larsen*, Jan. T. Ravnkilde**, Morten Ginnerup*, Ole Hansen*
MIC, Technical University of Denmark, 2800 Lyngby, Denmark*, Dicon A/S, Denmark**
E-mail: kpl@mic.dtu.dk

ABSTRACT

In-situ fatigue test devices with integrated electrostatic actuator were fabricated in electroplated nanocrystalline nickel (nano-nickel). The devices feature in-plane approximately pure bending with fixed displacement of the test specimen of the dimensions: widths from 2μm to 3.7μm, a height of 7μm and an effective length from 4μm to 27μm. Maximum stresses of the test beam were calculated to be 500MPa to 2100MPa by use of FEM tools. The test results indicate very promising fatigue properties of nano-nickel, as none of the test devices have shown fatigue failure or even initiation of cracks after 10^8 cycles. The combination of high strength and toughness, which is known for nanocrystalline materials, together with very small test specimens and low surface roughness could be the explanation for the good fatigue properties.

INTRODUCTION

Fatigue properties of MEMS materials are very important for the further development of MEMS. Polysilicon has been offered the most systematic research [1, 2, 3, 4, 5]. This work uses nanocrystalline nickel (nano-nickel) with grain sizes estimated to 100nm. Compared to the brittle polysilicon, nano-nickel offers very different mechanical properties and aging behavior, which has not been investigated much from a micromechanical point of view. A popular way for obtaining fatigue data is the resonant aging method. Much focus has also been on using high resolution external micro actuation machines [6, 7]. Fatigue data can be obtained from test situations, which are similar to those present in MEMS applications, but it often does not give general information. Obtaining and mapping the the fatigue properties in a standardized and reproducible way is difficult due to several factors: 1) The dimensions and surface finish of the test specimen should be well-known, and should ideally be of standardized geometries to avoid scaling effects. 2) The applied load or strain is mostly high and should also well-be known. 3) A numerous number of tests must be performed in order to achieve a statistical data set, and each test may be very time demanding. 4) Testing should be done in a controlled environment, especially temperature and humidity may have strong influences.

In this work released micromechanical structures have been fabricated using electroplated nickel from a sulphamate bath. The fabrication is a true low temperature process($\leq$ 140°C), and is optimized for CMOS compatible post processing [8].

The plating method used results in a grain size of 100nm, and can be characterized as nanocrystalline. The electroplated nickel can be deposited with practically no residual stress (below 10MPa). A lot of interest has been shown to nano-nickel in the material research [9, 10, 11, 12] but only few investigations has been done from a micromechanical approach. Decreasing the grain size yields in many ways an optimal improvement of the mechanical properties. This is due to a simultaneously increase of strength and fracture toughness. Tensile tests on nickel with 30nm grains [11] showed an improved ultimate tensile strength of 1.5GPa, and $\sigma_{0.2\%}$ of 1.0GPa which is a significant improvement to conventional nickel, which has 500MPa and 300MPa respectively. Compared to conventional nickel the ductility was reduced. The test showed a decreased linear elastic region (difficult to define Young's modulus), and a dependency of the strain rate by which the test was performed. Generally an increased creep behavior at low temperatures is observed[11, 12]. Grain growth at relatively low temperatures, reported for very fine grained nano-nickel [10, 13], could also represent a draw-back. The fatigue properties of nano-nickel are only sparsely investigated [14]. Investigations and theory agree on that a reduction of the grain size and the surface roughness will lead to increased initiation periods for fatigue cracks.

THE DEVICE

A SEM image of a representative device is shown on Fig. 1. The fabricated device features a compact *in-situ* measurement of an in-plane bending of an uncracked specimen with integrated electrostatic actuation giving a fixed maximum displacement. Electronic fracture detection is possible and parallel connection of the devices enables running several tests simultaneously. The test beam is situated in the upper left corner of the device. The test beam has a mean width of approx. 3μm and is 7μm thick. The length of the test beam, L_b is varied from 7μm to 30μm, as seen on

0-7803-7185-2/02/$10.00 ©2002 IEEE

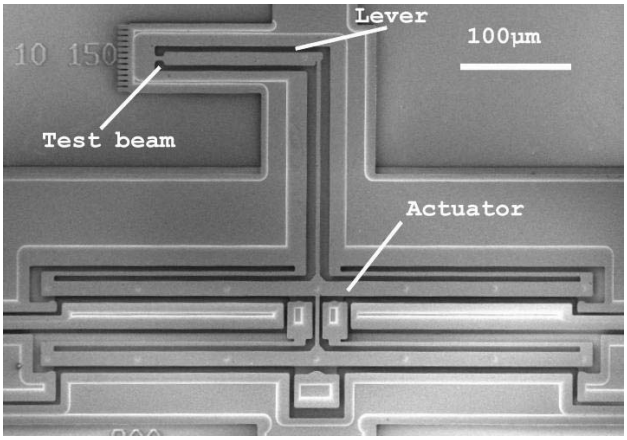

Figure 1: SEM image of a representative device, showing the important elements.

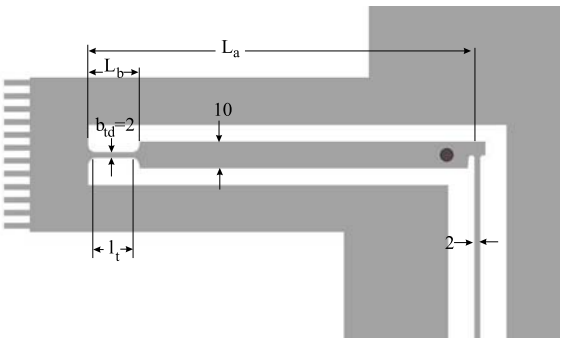

Figure 2: Design dimensions for the test beam and lever part. Dimensions in microns. The black spot is a bump, used to prevent stiction during fabrication.

Fig. 2. L_b corresponds to a smaller effective length l_t which is estimated to $l_t \approx L_b - 3\mu$m. The test beam is fixed at the left end and connected to a lever at the other end. The end of this lever is displaced by the long thin beam connected to the double electrostatic actuator mechanism, see Fig. 3. Applying a voltage across the moveable and fixed electrodes gives an electrostatic attraction, which eventually leads to pull-in. Bumpers prevent a short circuit, and leaves a 2μm gap between the actuator electrodes, see Fig. 4. The voltage is applied across the top and bottom of the device. The pull-in displacement of the electrodes is approximately 4μm. Spring beams connected to the electrodes and the compliance of the test beam bring the displacement back to the initial state when the voltage is zero. Some of the devices were designed with a separate connection to one set of the bumpers. This can be used for electronic fracture detection. Variations of the current design were stepped out in a large number on a wafer (9 variants, each in 21 copies). The devices can be connected in parallel, whereby it is possible to perform tests on several devices simultaneously.

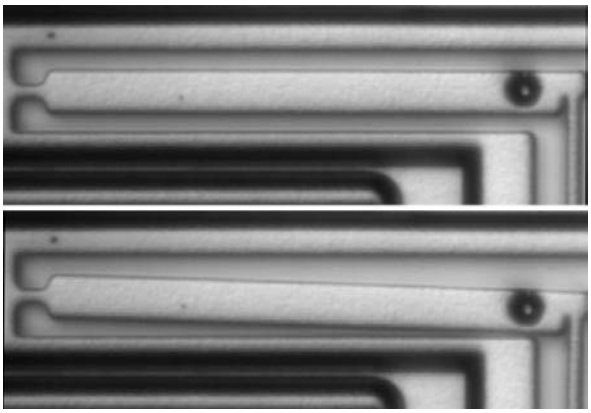

Figure 3: The test section and lever in relaxed (top) and maximum (bottom) displacement conditions.

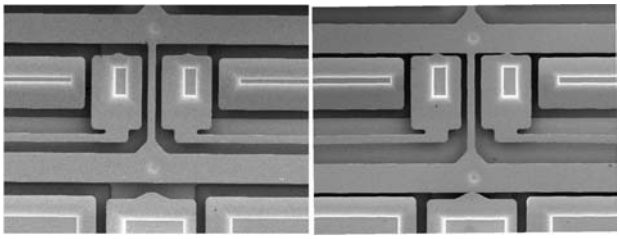

Figure 4: SEM image of the center part of the actuation electrodes, showing relaxed state (left) with 6μm gap between electrodes and full displacement (right), where bumpers leave a gap of 2μm between the electrodes.

FABRICATION

The process sequence for fabrication of the devices is shown in Fig. 5. The structures are made in a 4 mask process. First, a structured thin metal layer is formed on an oxidized 4 inch silicon wafer, Fig. 5A-5B. The layer is formed by e-beam evaporation and lift-off of a bi-layer of Cr/Ni of thickness 200Å/1500Å. This layer serves as an electrostatic shield between the test structures and the silicon substrate. In the next step, a seed layer of Ti/Au, of thickness 200Å/1500Å, is deposited by e-beam evaporation. Then, a 4μm thick sacrificial copper layer is electroplated in a photoresist mould, defined by the Anchor mask, Fig. 5C. In this Cu layer, bumps are etched using a photoresist mask, Fig. 5D. Hemi-spherical bumps, approximately 1μm deep, are obtained using an Ammonium-peroxydisulphate etch (25g/l) for 2.5min. The bumps are used to prevent stiction during the subsequent release etch of the structures. A final photoresist mould is defined and used for defining the 7μm thick structural electroplated nickel layer, Fig. 5E. This layer is electroplated at 40°C in a nickel sulphamate bath at a current density of 3A/dm^2. The plating bath is optimized for very low residual stress and small grain size ($\sim$ 100nm). Finally, the structures are released by se-

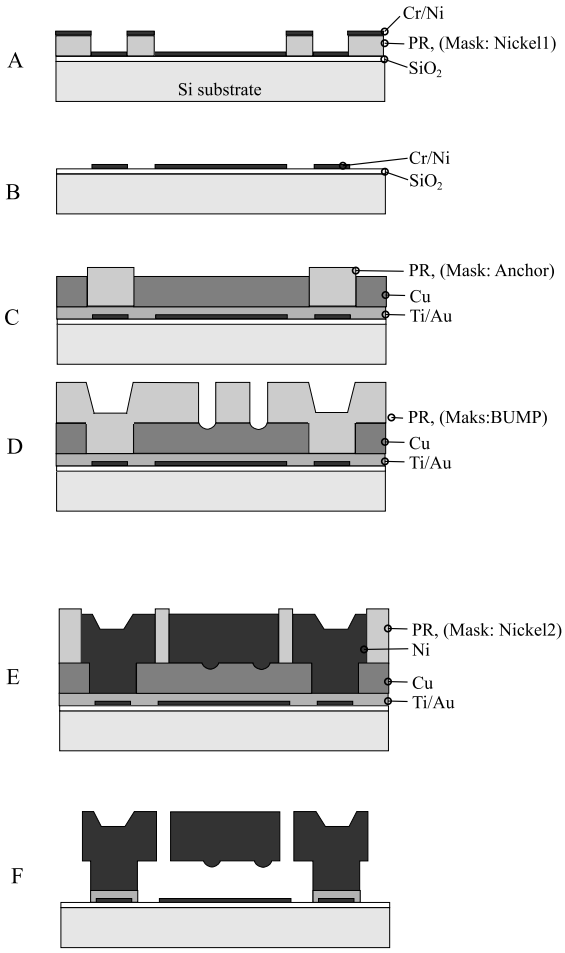

Figure 5: Fabrication process sequence.

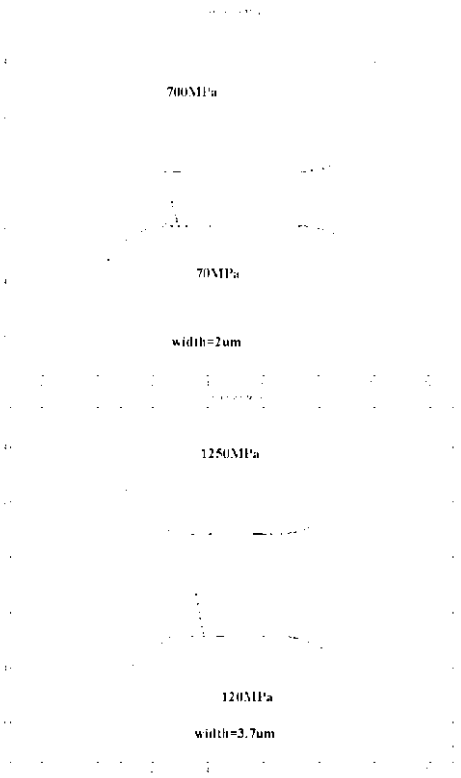

Figure 6: Different plane sections of the same device L_a=150μm, L_b=10μm and a thickness of 7μm. a) In the bottom surface the structures have approximately the same dimensions as designed. b) Due to line broadening (+0.85μm) the upper surface has much higher stress levels under deformation.

lective etching of copper, gold and titanium, and dried in ethanol.

FEM CALCULATIONS

The stress and strain in the fabricated test section were analyzed with 2D and 3D FEM tools. The excitation of the test beam is approximately pure bending, corresponding to an acting moment at the right-hand end of the test specimen. Considerable stress concentrations only occur in the test beam. Depending on the length of the test beam different max stresses were obtained. The beam has a slightly trapezoid cross section, giving a line broadening effect which adds +0.85μm to each edge for a thickness of 7μm. The highest stress levels are found at the upper surface where the beam is widest. Fig. 6 shows the von Mises stress levels at the upper and lower surface of a test specimen with L_b=10μm and L_a=150μm and a displacement at the end of the lever of 4μm. Maximum tensile stress levels are found locally as indicated on the figure, but drops steeply with a gradient in the order of 700MPa/μm. It should be noted that the stress levels are sensitive to small changes of the dimensions of the test beam geometry. Fig. 7 shows an overview of the calculated maximum stress levels for the 9 fabricated device variations. The upper curve corresponds to upper surface, and lower curve is the lower surface. During operation of the test device, the test beam is exposed to a pulsed stress excitation, alternating between relaxed stress free state and maximum stress levels.

SETUP AND TESTING

All the device variants operated satisfactorily, with pull-in voltages, V_p, of approximately 250V for the stiffest and at 190V for the softest devices. This is in good agreement with the expected values. The setup for cyclic testing is shown in Fig. 8, where two devices are tested simultaneously. Resistors of 100kΩ protects the devices from meltdown in case of a short circuit. The connection to the devices was done with a probe station in ambient environment. Detection of fracture of the test beam was here done by visual inspection. The applied bias voltage, V_{dc} and AC voltage, V_{ac} were adjusted to ensure full amplitude on all devices. The frequency used was from 10Hz to 500Hz. Mostly 200Hz was used.

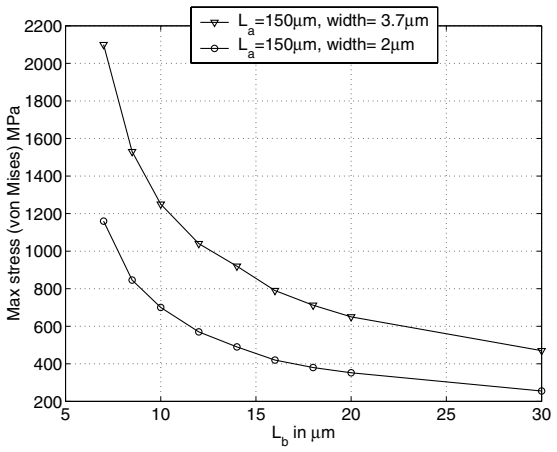

Figure 7: Calculated maximum von Mises stresses at a displacement of 4μm. The upper curve is the stress in the top surface of the bend beam. The lower curve is the stress in the bottom surface.

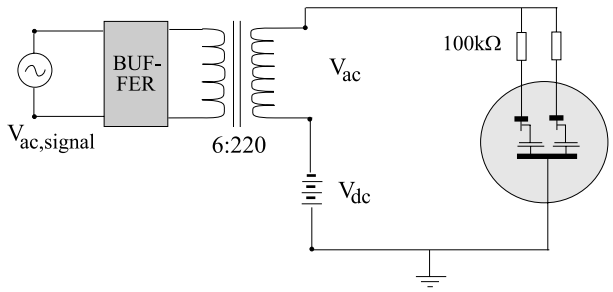

Figure 8: Diagram of the fatigue testing setup.

RESULTS AND DISCUSSION

An unexpected 'problem' became progressively apparent during the testing as none of the devices ever suffered from fatigue fracture. Two of the devices with highest maximum stress levels (2100-1150MPa), L_a=150μm and L_b=7μm were tested simultaneously, and both survived more than $1.1{\cdot}10^8$ cycles at a frequency of 200Hz. The initial value of the pull-in voltage for these devices were 252V, but dropped to 247V during the first 3 cycles. During the testing V_p decreased further to 226V at 10^7 cycles and 216V at 10^8 cycles. A slight permanent bending of the lever was observed, which may explain the lowering of the pull-in voltages. The number of cycles at the applied excitation of the test beam is apparently below the fatigue limit. The decrease of V_p indicates plastic deformations in the test beam, which is partly initiated during the first cycles but evolves further, indicating cyclic creep. A long initiation period is expected due to low surface roughness and nanocrystalline microstructure yielding high toughness and strength. High stress gradients normally inhibit and restrict the growth of cracks. Improvements to the design are underway, including symmetric load conditions, and larger displacements amplitudes.

CONCLUSION

The new test devices showed full functionality and operated as planned. The nano-nickel did not suffer from fatigue damage with the current devices. The results indicate promising fatigue properties for the use of nano-nickel in MEMS. Some plastic deformation and creep occurred, but no crack initiations was observed even after 10^8 cycles with calculated max. stresses of 2100-1150MPa. Several factors seem to contribute to improving the overall fatigue properties of micromechanical devices.

References

[1] T. Yi and C-J. Kim. Measurements of mechanical properties for mems materials. *Meas. Sci. Technol.*, 10:706–716, 1999.

[2] M. P. deBoer, B. D. Jensen, and F. Bitsie. A small area in-situ mems test structure to measure fracture strength by electrostatic probing. *Part of the SPIE Conference on Materials and Device Characterization on Micromachining II, sept 1999*, SPIE vol 3875:97–102, 1999.

[3] T. Ando, M. Shikida, and K. Sato. Tensile-mode fatigue testing of silicon films as structural materials for mems. *Sensors and Actuators A*, A 93:70–75, 2001.

[4] H. Kapels, R. Aigner, and J. Binder. Fracture strength and fatigue of polysilicon determined by a novel thermal actuator. *IEEE Transactions on electron devices*, 47(7):1522–1528, 2000.

[5] L. Que, L. Otradovec, A.D.Oliver, and Y. B. Gianchandani. Pulse and dc operation lifetimes of bent-beam electrothermal actuators. *0-7803-5998-4/01, IEEE*, 2001.

[6] S. Maekawa, K. Takashima, M. Shimojo, Y. Higo, S. Sugiura, B. Pfister, and M. V. Swain. Fatigue test of ni-p amorphous alloy microcantilever beams. *Jpn. J. Appl. Phys.*, 38:7194–7198, 1999.

[7] M. A. Haque and M. T. Saif. Microscale materials testing using mems actuators. *J. Microelectromechanical systems*, 10(3):146–152, 2001.

[8] Jan Tue Ravnkilde. *Metallic Microdevices for Monolithic Integrated Mocrosystems*. PhD thesis, Technical University of Denmark, Mikroelektronik Centret, 2800 Lyngby, 2000.

[9] F. Ebrahimi, G. R. Bourne, M. S. Kelly, and T. E. Matthews. Mechanical properties of nanocrystalline nickel produced by electrodeposition. *NanoStructured Materials*, 11(3):343–350, 1999.

[10] M. C. Iordache, S. H. Whang, Z. Jiao, and Z. M. Wang. Grain growth kinetics in nanostructured nickel. *NanoStructured Materials*, 11(8):1343–1349, 1999.

[11] W. M. Yin, S. H. Whang, R. Morshams, and C. H. Xiao. Creep behavior of nanocrystalline nickel at 290 and 373 k. *Material Science and Engineering*, A2301:18–22, 2001.

[12] Ning Wang, Zhirui Wang, K. T. Aust, and U. Erb. Room temperature creep behavior of nanocrystalline nickel produced by an electroplating technique. *Material Science and Engineering*, A237:150–158, 1997.

[13] Ning Wang, Zhirui Wang, K.T. Aust, and U. Erb. Isokenitic analysis of nanocrystalline nickel electrodeposits upon annealing. *Acta Mater*, 45(4):1655–1669, 1996.

[14] D. J. Morrison and J. C. Moosbrugger. Effect of grain size on cyclic plasticity and fatigue crack initiation in nickel. *Int. J. Fatigue*, 19(1):S51–S59, 1997.